NMR Studies of *Fusarium solani pisi* Cutinase in Complex with Phosphonate Inhibitors†

Jeanine J. Prompers,‡ Brigitte van Noorloos,‡ Maurice L. M. Mannesse,§,|| Anneke Groenewegen,§ Maarten R. Egmond,§,⊥ Hubertus M. Verheij,||,# Cornelis W. Hilbers,‡ and Henri A. M. Pepermans*,§

NSR Center for Molecular Structure, Design and Synthesis, Laboratory of Biophysical Chemistry, University of Nijmegen, Toernooiveld, 6525 ED Nijmegen, The Netherlands, Unilever Research, Olivier van Noortlaan 120, 3133 AT Vlaardingen, The Netherlands, and Department of Enzymology and Protein Engineering, CBLE, Utrecht University, Padualaan 8, 3584 CH Utrecht, The Netherlands

Received January 7, 1999; Revised Manuscript Received March 5, 1999

ABSTRACT: The backbone dynamics of *Fusarium solani pisi* cutinase in complex with a phosphonate inhibitor has been studied by a variety of nuclear magnetic resonance experiments to probe internal motions on different time scales. The results have been compared with dynamical studies performed on free cutinase. In solution, the enzyme adopts its active conformation only upon binding the inhibitor. While the active site Ser^{120} is rigidly attached to the stable α/β core of the protein, the remainder of the binding site is very flexible in the free enzyme. The other two active site residues Asp^{175} and His^{188} as well as the oxyanion hole residues Ser^{42} and Gln^{121} are only restrained into their proper positions upon binding of the substrate-like inhibitor. The flap helix, which opens and closes the binding site in the free molecule, is also fixed in the cutinase−inhibitor complex. Our results are in contrast with the X-ray analysis results, namely that in the protein crystal, free cutinase has a well-defined active site and a preformed oxyanion hole and that it does not need any rearrangements to bind its substrate. Our solution studies show that cutinase does need conformational rearrangements to bind its substrate, which may form the rate-limiting step in catalysis.

Cutinases are lipolytic enzymes capable of degrading cutin (*1*), the insoluble lipid−polyester matrix covering the surface of plants. They are produced by several phytopathogenic fungi and pollen, enabling them to gain entry into the plant by enzymatic digestion of its cuticle. Moreover, these enzymes, like lipases, catalyze the hydrolysis of ester bonds of triglycerides (*1*−*3*). In contrast to true lipases (*4*), however, *Fusarium solani pisi* cutinase shows no enhancement of its activity in the presence of a lipid−water interface (*2*, *3*). This phenomenon was rationalized by crystallographic studies of free cutinase from *F. solani pisi*, which revealed that it does not possess a pronounced lid covering the binding site like true lipases, but that it has an accessible active site with a preformed oxyanion hole (*5*−*7*). This suggested that in cutinase no significant rearrangements are necessary for substrate binding, whereas true lipases need a significant rearrangement of the lid to be able to bind their substrate (*8*−*10*). This hypothesis was subsequently confirmed by X-ray studies of cutinase−inhibitor complexes (*6*, *11*).

An enzyme that requires internal mobility for its activity may be forced into one conformation by the crystallization process (*12*). Because of this drawback of X-ray crystallography, we studied *F. solani pisi* cutinase in solution by NMR[1] (*13*). ^{15}N NMR relaxation and deuterium exchange studies revealed that the core of cutinase is highly rigid (*14*). However, in contrast to the X-ray analysis results, its binding site, including the oxyanion hole, appeared to be mobile on the microsecond to millisecond time scale in solution. The observed mobility most likely represents the interconversion between open and more closed conformations. The flap helix seemed to move as a whole, thereby opening and closing the binding site, like in a true lipase (*8*−*10*). The opening and closing motions are on a time scale which corresponds with the kinetics of the hydrolysis reaction, that is, the millisecond range (*3*). As an alternative explanation for the lack of interfacial activation, we proposed that, in contrast to true lipases, the open conformation of cutinase is not stabilized by an interaction between the lid and the remainder of the protein, so it closes and reopens between catalytic cycles (*14*).

To elucidate the effect of substrate binding on the dynamics of cutinase in solution, we performed NMR studies on this enzyme in complex with (*R*)-1,2-dibutyl-carbamoylglycero-3-O-*p*-nitrophenyl-butylphosphonate (TC4; ref *15*). TC4 is a triglyceride analogue, in which two of the ester bonds have been replaced by nonhydrolyzable carbamates and the third acyl ester group has been replaced by a *p*-nitrophenyl-alkylphosphonate. TC4 forms a covalent complex with cutinase, which mimics the first tetrahedral

† J.J.P. was supported by a grant from Unilever Research (URV 10087).

* Corresponding author. Tel: 31-10-4605508. Fax: 31-10-4605192. E-mail: Rik.Pepermans@Unilever.com.

‡ University of Nijmegen.

§ Unilever Research.

|| Current address: Leiden Institute of Chemistry, University of Leiden, Einsteinweg 55, 2300 RA Leiden, The Netherlands.

⊥ Utrecht University.

Deceased on August 1, 1998.

[1] Abbreviations: NMR, nuclear magnetic resonance; TC4, (*R*)-1,2-dibutyl-carbamoylglycero-3-O-*p*-nitrophenyl-butylphosphonate; TPPI, time proportional phase incrementation; HSQC, heteronuclear single-quantum coherence spectroscopy; FHSQC, fast HSQC; NOESY, nuclear Overhauser enhancement spectroscopy; TOCSY, total correlation spectroscopy; NOE, nuclear Overhauser effect; CSA, chemical shift anisotropy; CW, continuous wave; ROESY, rotating-frame Overhauser enhancement spectroscopy; ROE, rotating-frame Overhauser effect.

10.1021/bi990039k CCC: $18.00
Published on Web 04/20/1999

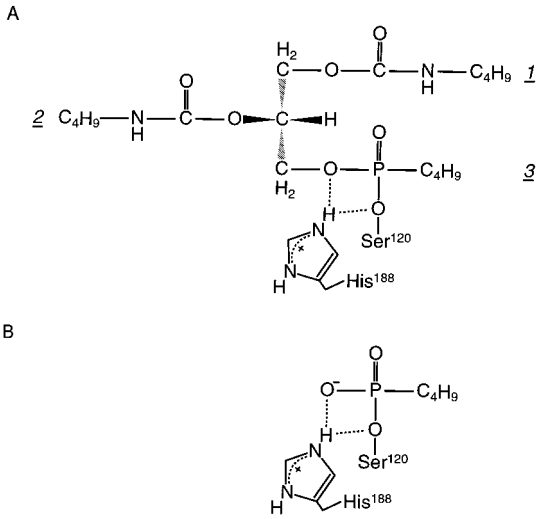

FIGURE 1: Chemical structure of (A) TC4 bound to the catalytic serine and (B) the reaction product after aging. In panel A the numbering of the chain positions is indicated by the underlined, italic numbers.

intermediate along the reaction pathway with 1-2-dihexanoyl-3-pentanoyl-glycerol (Figure 1A). Unfortunately, this complex appeared to decompose during the time course of the NMR experiments due to an aging reaction, which has also been described for, for example, cholinesterase (*16*, *17*) and *Pseudomonas cepacia* lipase (*18*). During the aging process, the dicarbamoyl−glycerol moiety is split off, but the butylphosphonate remains bound to the active site serine (Figure 1B) while the phosphonyl oxygen should still fill the oxyanion hole. Dynamical studies were performed on this aged cutinase−TC4 complex.

Another aspect of this study concerns the observed effects of acyl chain length and position in the substrate molecule on the activity and enantioselectivity of *F. solani pisi* cutinase (*19*). Kinetic studies with pseudo triglycerides containing only one hydrolyzable ester bond at the 3-position showed that the activity of cutinase is very sensitive to the length of the chain that is hydrolyzed, as well as to that of the chain at the 1-position: The highest activities were found when the chains at positions 1 and 3 contain three or four carbon atoms. Furthermore, it was shown that cutinase preferentially hydrolyzes the (*R*)-enantiomers of these pseudo triglycerides (which are chiral on the central carbon of the glycerol moiety), corresponding to the hydrolysis of the *sn*-3 ester in natural triglycerides, and that the extent of the enantioselectivity depends on the length of the chains at the 1- and 2-positions. The crystal structure of the cutinase−TC4 complex (*11*) only provided a structural explanation for the preference of cutinase for short chains at the 3-position, that is, the scissile acyl chain. The chain at this position is completely buried in a rather small pocket. Only about five carbon atoms can be embedded in this pocket, which explains the drop in activity when using longer ester chain substrates. However, the X-ray structure cannot explain the effect of the chain length at the 1-position on the activity, neither can it explain the enantioselectivity, because both the chains at the 1- and 2-position protrude from the protein. In the crystal structure, two cutinase−TC4 complex molecules face each other head-to-head and part of the inhibitor has interactions with the neighboring cutinase molecule and its bound inhibitor. The obtained conformation might thus be an artifact of the crystallization process. We tried to elucidate whether the structure of the complex is different in solution and whether this structure can explain the enantioselectivity and chain-length selectivity of cutinase.

MATERIALS AND METHODS

Sample Preparation. Recombinant uniformly ^{15}N-labeled cutinase was produced in *Saccharomyces cerevisiae* as described elsewhere (*20*) modified by using ^{15}N-labeled ammonium sulfate (99% ^{15}N, Cambridge Isotope Laboratories) as the sole nitrogen source. The protein was purified as described previously (*21*). Lyophilized, uniformly ^{15}N-labeled cutinase was dissolved in buffer containing 10 mM deuterated sodium acetate (99.5% D), 100 mM NaCl, and 0.02% sodium azide, pH 5.0. The H_2O samples were 95% H_2O/5% D_2O (99.9% D), and the D_2O sample was 100% D_2O (99.9% D). For the D_2O sample, the pH meter readings were corrected for the isotope effect (*22*).

(*R*)-1,2-dibutyl-carbamoylglycero-3-O-*p*-nitrophenyl-butylphosphonate (TC4) was synthesized as described previously (*11*, *15*). Three H_2O samples of cutinase in complex with TC4 were prepared by adding a 10-fold excess of TC4 (dissolved in acetonitrile) to the protein solutions, which were then incubated overnight at room temperature. The completion of the inhibition was checked by measuring the remaining activity on *p*-nitrophenylbutyrate. The vast excess of (insoluble) inhibitor and some precipitated protein were removed by centrifugation. Two of the samples, containing 0.25 and 0.45 mM cutinase, respectively, were directly subjected to NMR measurements to be able to observe signals from the fresh, unaged complex. After the measurements, these samples were stored until the aging reaction was completed (checked by NMR spectroscopy), pooled, desalted by gelfiltration on a PD-10 column (Pharmacia), and subsequently lyophilized. This lyophilized, aged cutinase−TC4 complex was used for the D_2O exchange experiments. The NMR spectra of the aged cutinase−TC4 complex in H_2O buffer were recorded two months after sample preparation, when the aging reaction was completed (checked by NMR spectroscopy). Before the NMR experiments, the acetonitrile, inhibitor, and aging products were removed by gel filtration on a PD-10 column (Pharmacia). The sample was subsequently concentrated to a concentration of 0.45 mM with a Centricon-10 concentrator (Amicon).

NMR Spectroscopy. All experiments were performed on a Bruker 600 MHz AMX spectrometer equipped with a Bruker BLAX 300 W linear amplifier and a 5 mm inverse triple-resonance probehead (^{1}H/^{15}N/^{13}C) with a self-shielded z-gradient coil. All experiments were carried out at 25 °C (console readout) to allow a comparison with the studies of the free enzyme, unless stated otherwise. The spectral width in the ^{15}N dimension was 1824 Hz (folding in some backbone resonances), and it was 7246 Hz in the ^{1}H dimension(s). The number of complex points, number of scans per FID, and number of points after processing of all spectra are listed in Table 1. Quadrature detection in the indirectly detected dimensions was accomplished using the States-TPPI acquisition method (*23*).

A 2D ^{15}N-^{1}H water flip-back fast HSQC (FHSQC; ref *24*), a 3D ^{15}N-edited NOESY−HSQC (*25*) with a mixing time of 75 ms, and two 3D ^{15}N-edited TOCSY−HSQC experiments using mixing times of 35 and 70 ms, respectively,

Table 1: Acquisition and Processing Parameters for the Various Experiments

		heteronucleus			no. of complex points				final spectrum size		
sample	experiment	F1	F2	F3	F1	F2	F3	scans	F1	F2	F3
aged complex (H_2O)	^{15}N-^{1}H HSQC	^{15}N	^{1}H		256	1024		80	1024[a]	600[b]	
	^{15}N NOESY-HSQC	^{15}N	^{1}H	^{1}H	30	96	1024	16	128[a]	256[a,c]	600[b]
	^{15}N TOCSY-HSQC	^{15}N	^{1}H	^{1}H	28	88	1024	16	128[a]	256[a,c]	600[b]
	R_1	^{15}N	^{1}H		256	1024		32	1024[a]	600[b]	
	R_2	^{15}N	^{1}H		256	1024		32	1024[a]	600[b]	
	$R_{1\rho}$	^{15}N	^{1}H		256	1024		32	1024[a]	600[b]	
	NOE + reference	^{15}N	^{1}H		256	1024		40	1024[a]	600[b]	
	water-NOESY	^{15}N	^{1}H		190	1024		128	1024[a]	600[b]	
	water-ROESY	^{15}N	^{1}H		190	1024		384	1024[a]	600[b]	
aged complex (D_2O)	^{15}N-^{1}H HSQC	^{15}N	^{1}H		128	1024		8	1024[a]	600[b]	
fresh complex (H_2O)[d]	^{15}N-^{1}H HSQC	^{15}N	^{1}H		256	1024		76	1024[a]	600[b]	
	^{15}N NOESY-HSQC	^{15}N	^{1}H	^{1}H	32	102	1024	16	64[a]	256[a,c]	600[b]
fresh complex (H_2O)[e]	^{15}N-^{1}H HSQC	^{15}N	^{1}H		256	1024		32	1024[a]	600[b]	
	^{15}N NOESY-HSQC[f]	^{15}N	^{1}H	^{1}H	32	116	1024	16	64[a]	256[a,c]	600[b]

[a] Number of points after zero-filling. [b] Number of points after extracting the H^N region. [c] Number of points after linear prediction. [d] Sample contains 0.25 mM cutinase. [e] Sample contains 0.45 mM cutinase. [f] Two NOESY spectra were added (see text).

were recorded on the aged cutinase−TC4 complex for assignment purposes. In the NOESY−HSQC sequence a gradient pulse was added at the end of the mixing time to remove nonzero order coherences (*26*). The TOCSY−HSQC sequence was based on the gradient-enhanced TOCSY experiment proposed by Fulton et al. (*27*), which was combined with the FHSQC sequence (*24*) in a manner identical to the NOESY−HSQC experiment.

For the assignment of the fresh complex, 3D ^{15}N-edited NOESY−HSQC experiments (*25*) with a mixing time of 100 ms were recorded on the fresh cutinase−TC4 samples, preceded and succeeded by 2D ^{15}N-^{1}H FHSQC's (*24*). The fresh complex has an approximate half-life of 4 days at pH 5.0 and 25 °C. The decay of the signals originating from the fresh cutinase−TC4 complex due to the aging process negatively affects the sensitivity of the 3D NOESY−HSQC experiment. This decay adds on top of the normal signal decrease due to relaxation most seriously for the "slowest" indirectly detected dimension, the ^{15}N dimension, resulting in very broad peaks for the fresh complex. Therefore, simply increasing the number of scans will not result in higher signal-to-noise ratios for the signals originating from the fresh complex. To circumvent this problem, we recorded two 3D NOESY−HSQC experiments sequentially: One normal, forward experiment and one backward experiment, in which we reversed the time in the indirect ^{15}N dimension. For the latter experiment, the signal decays due to aging and relaxation do not longer enhance each other. We added the forward and backward spectra after processing (forward/backward NOESY), resulting in higher signal-to-noise ratios for the signals originating from the fresh complex compared to a normal forward 3D NOESY−HSQC with a comparable total acquisition time.

The pulse sequences used to measure longitudinal (R_1) and transverse (R_2) relaxation rate constants, and ^{1}H-^{15}N steady-state nuclear Overhauser effects (NOEs) of the backbone ^{15}N nuclei of cutinase in the aged cutinase−TC4 complex were based on those of Kay et al. (*28*), modified to eliminate cross-correlation between dipolar and chemical shift anisotropy (CSA) relaxation (*29*−*31*). $R_{1\rho}$ measurements were essentially performed as described in Prompers et al. (*32*). The indirect nitrogen evolution period followed by the INEPT transfer was concatenated into a semiconstant time ^{15}N evolution period in all relaxation experiments. Gradients were used to suppress artifacts (*33*) and to aid in the removal of water by means of the WATERGATE sequence (*34*). In the R_1, R_2, and $R_{1\rho}$ experiments, additional water suppression was accomplished by high-power spin-lock pulses (*35*). A prescan recovery delay of 1 s was used for the R_1, R_2, and $R_{1\rho}$ experiments. For the R_1 measurements, spectra were recorded using relaxation periods of 4, 103, 203, 303, 403, 603, 803, 1003, 1303, and 1803 ms. The phase of the 90° pulse before the relaxation period was alternated between y and $-y$ to ensure that the magnetization relaxes as $\exp(-T/T_1)$ (*28*). For the R_2 experiments, spectra were recorded with relaxation periods of 3.5, 7.0, 10.5, 14.0, 21.1, 28.1, 42.1, 56.2, 70.2, 84.3, 119.4, and 165.1 ms consisting of Carr-Purcell-Meiboom-Gill pulse trains. For the $R_{1\rho}$ experiments, spectra were recorded with relaxation periods of 4, 8, 12, 16, 20, 28, 40, 60, 80, 100, 120, and 160 ms consisting of a CW spin-lock with a frequency of about 2.6 kHz. For the NOE experiments two spectra were recorded sequentially, one with and one without proton saturation. In the NOE experiment a decoupling sequence was applied for 7 s to saturate the ^{1}H resonances. This was replaced by a prescan recovery delay of the same length in the reference spectrum. Shorter recovery delays led to significant errors in some intensities of the reference spectra. NOE and reference measurements were repeated three times.

Water-NOESY and water-ROESY experiments were recorded on the aged cutinase−TC4 complex as modified versions of the HYDRA-N and HYDRA-R NOE difference experiments with diffusion filters for separation of water−protein and protein−protein NOEs (*36*). The basic one-dimensional HYDRA scheme was combined with the FHSQC experiment (*24*) to achieve spectral resolution. A prescan recovery delay of 2 s was used. Water-NOESY experiments were recorded with a mixing time of 100 ms at both 20 and 25 °C, and a water-ROESY was recorded with a 50 ms CW spin-lock period at 25 °C only.

Amide hydrogen exchange data were recorded on the lyophilized, aged cutinase−TC4 complex, immediately after dissolving it in D_2O buffer to a concentration of 0.5 mM at 25 °C and pH 5.0. In total, 38 ^{15}N-^{1}H FHSQC spectra were measured between 1 h and approximately one week after sample preparation.

Data Analysis. Spectra were processed and analyzed on Silicon Graphics workstations, using the Triad software package (Tripos Inc.). Convolution filtering of the time domain data with a Gaussian function was applied to the acquisition dimension of the spectra recorded in H_2O to suppress the water signal (*37*). All dimensions were apodized using a squared-cosine bell. Linear prediction (*38*) and/or zero-filling was used to improve the digital resolution (see Table 1). In all spectra, the empty right part of the acquisition dimension was discarded by extracting the amide region (see Table 1).

Weighted averages of amide ^{1}H and ^{15}N chemical shift differences were calculated according to Grzesiek et al. (*39*) as

$$\Delta\delta = [0.5(\Delta\delta_{HN}{}^2 + (\Delta\delta_N/5)^2)]^{1/2} \quad (1)$$

To visualize the effect of complexation on a CPK model of the crystal structure, we gave each atom a color index C_x, calculated from all weighted averages of the amide chemical shift differences and the distances of atom x to all amide groups:

$$C_x = \sum S_{NH} \exp(-k^{dist} r_{NH,x}) \quad (2)$$

in which $r_{NH,x}$ is the distance between atom x and the nitrogen atom of the amide group and k^{dist} is a distance factor, which was set to 0.6 Å^{-1}. S_{NH} is related to the weighted average of the amide ^{1}H and ^{15}N chemical shift differences defined by eq 1: S_{NH} was set to -1 when $\Delta\delta \leq 0.05$ ppm (no significant shift), to $+1$ when $\Delta\delta > 0.05$ ppm (significant shift), and to 0 for the amides for which $\Delta\delta$ could not be determined (prolines and the N-terminal arginine). For each atom, the summation runs over all amide groups. Atoms with $C_x \leq -1$ were colored blue, atoms with $C_x \geq +1$ were colored red, and atoms with $C_x = 0$ were colored white. For C_x values between -1 and 0 a color gradient was applied from blue to white, and for C_x values between $+1$ and 0 a color gradient was applied from red to white.

Relaxation rate constants and NOEs were calculated from peak volumes. The R_1, R_2, and $R_{1\rho}$ constants were obtained by fitting two-parameter single-exponential functions to the experimental data using the SAS package (SAS Institute Inc.), applying the Levenburg-Marquardt algorithm (*40*, *41*). Error estimates for the rates were obtained from the standard deviations of the curve fits. Heteronuclear NOEs were calculated as the ratios of peak volumes from the spectra recorded with proton saturation to those from the spectra recorded without saturation. Repeated NOE measurements were then averaged. The uncertainties were calculated from the standard deviations.

The effective relaxation rates in the rotating frame ($R_{1\rho}^{eff}$) are approximately a linear combination of R_1 and $R_{1\rho}$ due to resonance offset effects (*42*−*45*):

$$R_{1\rho}^{eff} = R_1 \cos^2\beta + R_{1\rho} \sin^2\beta \quad (3)$$

where $\cos\beta = \Delta\omega/\omega_e$, $\omega_e = (\Delta\omega^2 + \omega_{SL}{}^2)^{1/2}$, and $\Delta\omega$ is the offset between the spin-lock carrier and the resonance frequency. The ^{15}N spin-lock power ω_{SL} was set to 16.5×10^3 rad s^{-1}. The $R_{1\rho}$ values for all residues were calculated with eq 3, using experimental values of $R_{1\rho}^{eff}$ and R_1.

Table 2: The Different Models Used during the Model-Free Analyses

model	parameters	no. of residues (isotropic, $\tau_c = 9.68$ ns)	no. of residues (anisotropic, $\tau_c = 9.82$ ns)
1	S^2	118	152
2	S^2, τ_e	6	10
3	S^2, R_{ex}	46	11
4	S^2, τ_e, R_{ex}	2	1
5	$S_f{}^2$, $S_s{}^2$, τ_s	9	7

The ^{15}N relaxation data were analyzed in terms of the model-free model (*46*−*49*) by directly fitting the model-free parameters to the peak volumes from which the relaxation rates and the NOE are derived (*32*). Initially, a global value of τ_c was determined from the mean of the R_2/R_1 ratios of the most rigid core residues (*28*, *48*) using the following estimation (*50*):

$$\tau_c = (1/2\omega_N) \times [(6R_2/R_1) - 7]^{1/2} \quad (4)$$

where ω_N is the Larmor frequency of the ^{15}N nuclei. In addition, τ_c was estimated from the mean of the $R_{1\rho}/R_1$ ratios in the same manner. On the basis of the initial estimates from the R_2/R_1 and $R_{1\rho}/R_1$ ratios, several values between 9.00 and 11.00 ns were used as starting values for τ_c. It was then attempted to fit five different models (see Table 2). In all cases we selected the model with the fewest number of model-free parameters consistent with the experimental results within the estimated error as described in Prompers et al. (*32*). The relaxation data were interpreted using both the isotropic and the axially symmetric anisotropic model. R_2 as well as $R_{1\rho}$ data were used for the model-free analyses. As the vast majority of residues lacked significant differences between R_2 and $R_{1\rho}$ (vide infra), we assumed that the exchange contributions to both of them, if present, are equal.

Conformational exchange processes on a time scale slower than the frequency of the $R_{1\rho}$ spin-lock field were identified by calculating the difference between the ^{15}N R_2 and $R_{1\rho}$ relaxation rates (*51*).

Amide proton−deuterium exchange rate constants were derived from peak volumes. The rate constants were calculated by fitting a single-exponential decay function to the experimental data, using a three-parameter fit to the equation

$$I(t) = I_\infty + (I_0 - I_\infty)\exp(-k_{ex}t) \quad (5)$$

where $I(t)$ is the intensity at time t after addition of D_2O to the lyophilized protein, I_0 is the intensity at $t = 0$, I_∞ is the intensity at $t = \infty$, and k_{ex} is the observed exchange rate constant. The parameters were fit using the SAS package (SAS Institute Inc.), applying the Levenburg-Marquardt algorithm (*40*, *41*). For amide protons that did not exchange completely before the last experiment was finished, and for which I_∞ was not well-determined, the decay curve was fit using a final intensity of 0. Error estimates for the rates were obtained from the standard deviations of the curve fits. The intrinsic rate constants k_{rc} were obtained using the parameters from Bai et al. (*52*). Protection factors P were then calculated according to the following:

$$P = k_{rc}/k_{ex} \quad (6)$$

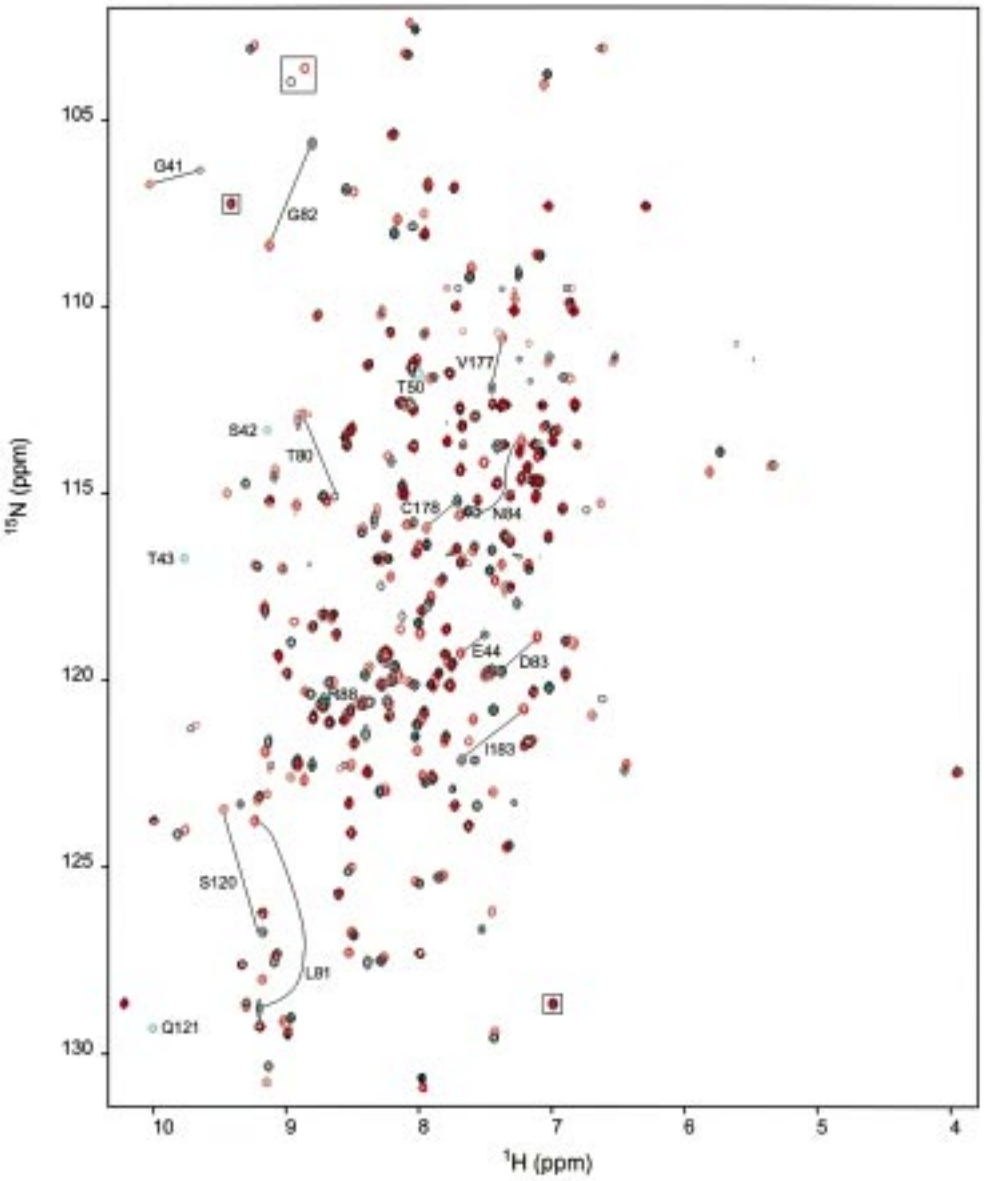

FIGURE 2: Overlay of the 2D ^{15}N-^{1}H HSQC spectra of free cutinase (black contours) and the aged cutinase−TC4 complex (red contours). The signals of Ser^{42}, Thr^{43}, Thr^{50}, Arg^{88}, and Gln^{121}, which are not visible for the free enzyme, are highlighted by the green contours in the spectrum of the aged complex, and their assignments are indicated using the one-letter amino acid code. Assignments are also indicated for those residues which shift most upon complexation. The peaks marked by boxes are backbone amide signals which are once folded in the ^{15}N dimension.

Mass Spectrometry. Unlabeled, inhibited cutinase samples were desalted by gel filtration on a PD-10 column (Pharmacia) and subsequently analyzed by electrospray mass spectrometry using a Quattro-II triple quadrupole mass spectrometer (Micromass).

RESULTS

Identification of the Complexes. It was shown by electrospray mass spectrometry that, upon inhibition of cutinase by TC4, initially the intact, fresh complex shown in Figure 1A is being formed. However, this complex appeared to decompose during the time course of our NMR experiments, giving rise to a new set of NMR signals in the ^{15}N-^{1}H HSQC spectrum. The decomposition is most probably due to an aging reaction, which has also been described for, for example, cholinesterase (*16*, *17*) and *Pseudomonas cepacia* lipase (*18*), leading to the formation of the aged complex depicted in Figure 1B. This was confirmed by electrospray mass spectrometry.

Assignment of the Cutinase−TC4 Complexes. F. solani pisi cutinase expressed in *Saccharomyces cerevisiae*, which was used in this study, consists of 198 residues. Compared to the protein produced in *Escherichia coli*, which was used for the studies of the free enzyme (*13*, *14*, *32*), it lacks the N-terminal propeptide (16 residues), which is not part of the mature enzyme. Apart from this difference, the ^{15}N-^{1}H HSQC spectra of both proteins are very similar and most of the backbone amide assignments for cutinase from *E. coli* (*13*) could be directly transferred to the enzyme produced in *Saccharomyces cerevisiae* (not shown).

The assignments of free cutinase served as a starting point for the assignment of the backbone amide resonances of the aged cutinase−TC4 complex. Shifted signals were identified with the help of the ^{15}N-edited TOCSY and NOESY spectra.

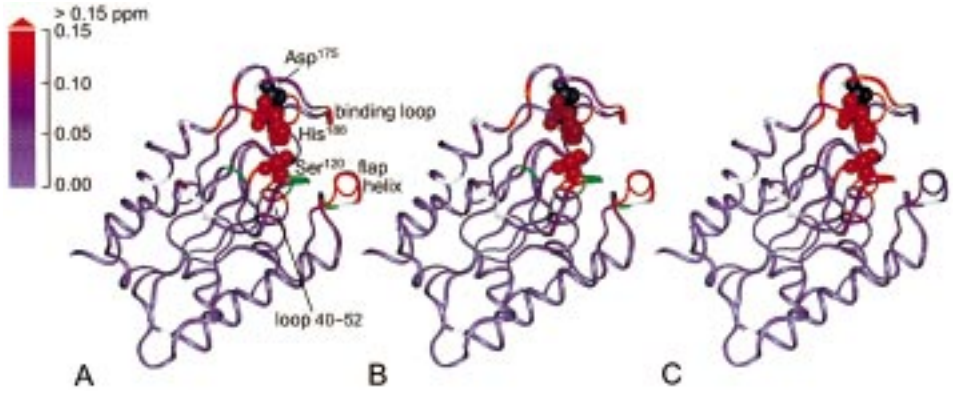

FIGURE 3: Weighted averages of the differences in amide ^{1}H and ^{15}N chemical shifts between (A) the fresh cutinase−TC4 complex and free cutinase, (B) the aged cutinase−TC4 complex and free cutinase, and (C) the fresh and the aged cutinase−TC4 complex, mapped on the crystal structure of the free protein (*5*). The five residues which have not been assigned in the free enzyme, Ser[42], Thr[43], Thr[50], Arg[88], and Gln[121], are colored green in parts A and B. Prolines and the N-terminal arginine, for which the difference could not be determined, are colored white. The active site residues are shown in space-filling representations. This figure was generated with the program Insight II (MSI).

All backbone amide resonances of the aged complex could be assigned. For the free enzyme, 5 residues (Ser[42], Thr[43], Thr[50], Arg[88], and Gln[121]) remained unidentified in the ^{15}N-^{1}H HSQC spectrum due to exchange broadening (*13*). In contrast, all expected correlations could be observed in the HSQC spectrum of the aged complex, including the signals of these five residues (Figure 2).

The backbone amide resonances of the fresh cutinase−TC4 complex were assigned using the assignments of the aged complex as a starting point. Shifted resonances were identified with the help of the ^{15}N-edited forward/backward NOESY spectrum. Furthermore, the ratio of the peak volumes in the ^{15}N-^{1}H HSQC spectra recorded before and after the normal, forward 3D ^{15}N-edited NOESY spectrum, which took about the half-life time of the aging process, aided in the assignment of the fresh complex. All backbone amide resonances of the fresh cutinase−TC4 complex could be assigned. The assignments of both the aged and the fresh cutinase−TC4 complex are listed in the Supporting Information.

Comparison of Backbone Amide Resonances. From Figure 3A,B it can be seen that the amide chemical shifts of the residues located in or around the binding site are most affected by complexation. For both the fresh and the aged cutinase−TC4 complex the largest differences from the free enzyme are found in the same regions and also the magnitudes of the averaged amide chemical shift differences are similar. The signals of the residues in the core and the loops at the other side of the molecule do not shift significantly upon inhibitor binding.

The amide chemical shift differences between the fresh and the aged complex give direct information on changes in the magnetic environment of the amides due to the presence or absence of the dicarbamoyl−glycerol moiety, which is split off during the aging process. These changes might be caused by a direct interaction with this part of the inhibitor, by a conformational change induced by this part of the inhibitor, or by a combination of both. The amide chemical shift differences between the fresh and the aged cutinase−TC4 complex could therefore give a clue as to the position of (one of) the two carbamoyl chains in solution. The largest shifts are found in the same regions as in the comparisons with the free enzyme, and the magnitudes of the averaged differences are also similar (Figure 3C). There is one exception: The amide resonances of the residues in the flap helix 81−85 are not affected by the aging process. In the crystal structure of the cutinase−TC4 complex (*11*), this helix binds the chain at the 3-position, which is still present after aging.

^{15}N Relaxation Rates. Among the 188 residues in the aged cutinase−TC4 complex which give rise to backbone signals in a ^{15}N-^{1}H HSQC spectrum (excluding the 9 prolines and the N-terminal arginine), 7 residues were excluded from the relaxation rate analysis due to resonance overlap (Ala[56], Leu[59], Gly[72], Arg[88], Asp[139], Asn[155], and Arg[211]). Thus, quantitative R_1, R_2, $R_{1\rho}$, and heteronuclear NOE measurements were made for 181 of the amide cross-peaks in the aged cutinase−TC4 complex. The relaxation rates and NOEs are shown in Figure 4. R_1, R_2 (except for Gly[89], Ser[91], and Gly[174]), $R_{1\rho}$ (except for Gly[89] and Gly[174]), and the heteronuclear NOEs are quite uniform for the core of the protein. The 3 residues at the C-terminal end have substantially deviating R_1, R_2, $R_{1\rho}$, and NOE values.

Model-Free Analysis of ^{15}N Relaxation Data. The global value of τ_c initially determined from the mean of the R_2/R_1 ratios of the most rigid core residues using eq 4 was 9.86 ± 0.59 ns. Ser[91] and Gly[174] were excluded from this calculation, as they obviously have significant exchange contributions to their R_2 (see Figure 4). Gly[89] was excluded because of its deviating R_2 value, probably due to some overlap with Thr[80]. In addition, the 3 residues at the C-terminal end were excluded, since the assumption of negligible τ_e values is clearly inappropriate for these highly mobile residues. The global value of τ_c determined from the mean of the $R_{1\rho}/R_1$ ratios was 9.72 ± 0.61 ns, which is only slightly lower than the value calculated from the R_2/R_1 ratios.

As a first approach, the model-free analysis was performed with the assumption that the aged complex of cutinase with TC4 tumbles isotropically. Using starting values for τ_c between 9.00 and 11.00 ns, the fit converged to a single minimum at an overall rotational correlation time of 9.68 ns. The number of residues fit to the different models is given in Table 2, and the parameters as obtained from the model-free analysis are listed in the Supporting Information.

As was observed for the free enzyme from *E. coli* (*32*), many residues in the α-helices covering the central parallel β-sheet needed an exchange contribution as they required

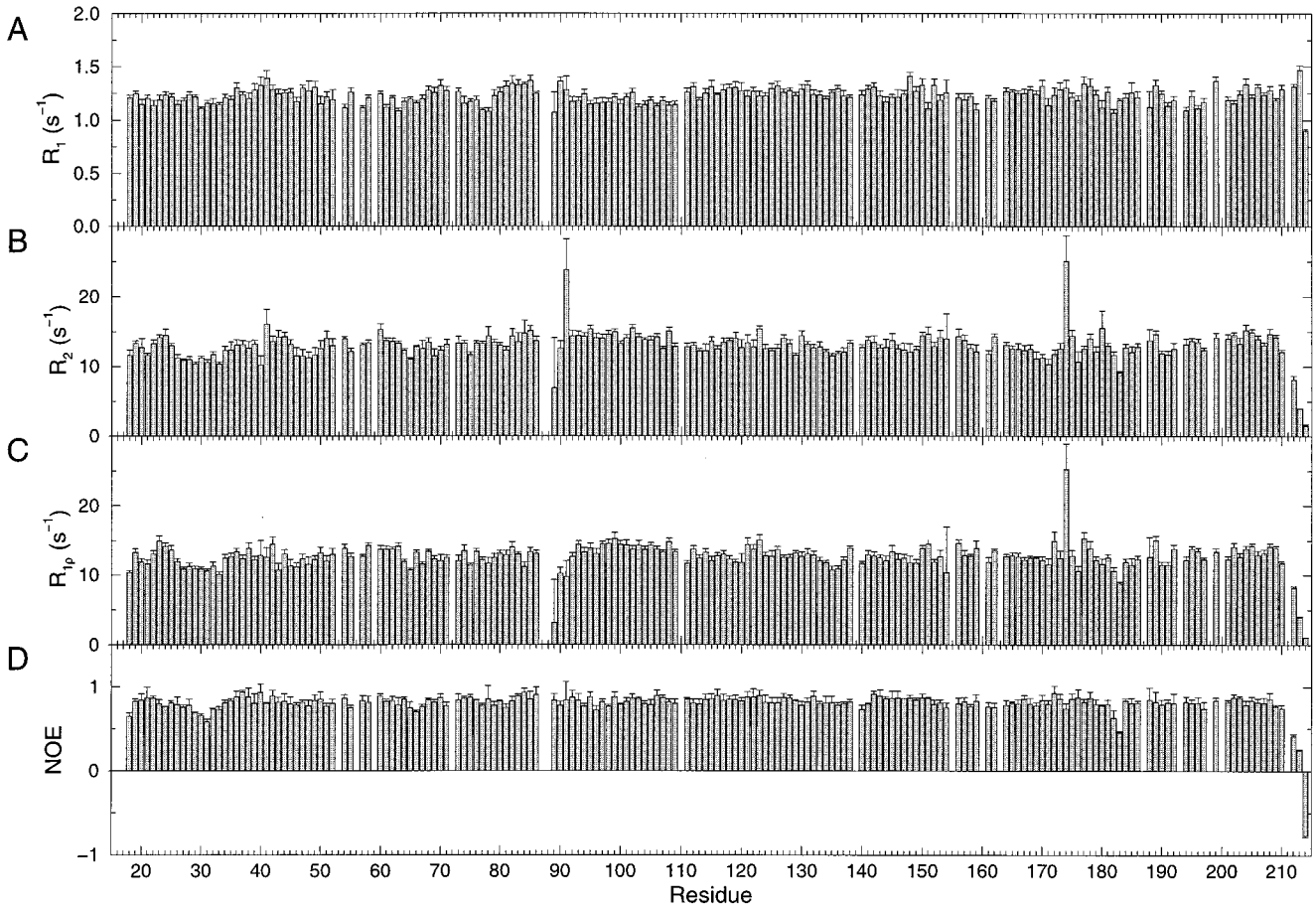

FIGURE 4: Backbone ^{15}N relaxation data: (A) R_1, (B) R_2, (C) $R_{1\rho}$, and (D) heteronuclear NOE as a function of the residue number of the aged cutinase−TC4 complex determined at 14.1 T.

fitting to model 3 (see Table 2). For free cutinase it was shown that these exchange terms were actually caused by the misinterpretation of anisotropic rotational diffusion (*32*). Like the free enzyme, the aged complex can be approximated by an axially symmetric rotor with a ratio of 1.3 for the rotational diffusion coefficients parallel ($D_{\|}$) and perpendicular ($D_{\perp}$) to the unique axis of the molecule. In Figure 5, experimental R_1 and $R_{1\rho}$ combinations of the aged complex are shown for residues in two major α-helices with their N−H vectors running nearly parallel to the long axis of the molecule and for residues in the β-sheet with their N−H vectors nearly orthogonal to the long axis of the molecule. The experimental values are covered by a grid of R_1 and $R_{1\rho}$ combinations predicted for a protein with an (effective) overall rotational correlation time of 9.68 ns. Combinations of R_1 and $R_{1\rho}$ values are given for different values of (1) S^2 and the internal correlation time when isotropic tumbling is assumed, (2) S^2 and the exchange contribution when isotropic tumbling is assumed, and (3) S^2 and the angle between the N−H internuclear vector and the unique axis of the molecule when anisotropic rotational diffusion is taken into account with a ratio $D_{\|}/D_{\perp}$ of 1.3. We introduced such a plot as a general tool to examine whether for an arbitrary protein anisotropic tumbling has to be included in the derivation of the motional parameters (*32*). The amide groups in the helices and in the sheet cluster into different regions of the plot, which clearly indicates that anisotropic tumbling should be taken into account in the interpretation of the relaxation data of the aged complex, just as for the free enzyme.

When treating the aged cutinase−TC4 complex as an axially symmetric rotor, the fit converged to a single minimum at an effective overall rotational correlation time of 9.82 ns. This value shows that the complex is monomeric in solution, just like the free enzyme. The number of residues fit to the different models when including anisotropy is given in Table 2, and the parameters as obtained from the model-free analysis are shown in Figure 6. Taking anisotropic tumbling into account hardly influenced the values of the overall rotational correlation time, the order parameters, or the internal correlation times. In contrast, introduction of anisotropic tumbling had a large effect on the exchange contributions. For 38 residues, mainly located in the helices running parallel to the longest axis of the molecule, the exchange term could be omitted, while for only 2 residues (residues 44 and 68) an exchange term had to be included.

Apart from the C-terminus, only three loop regions (residues 27−33, 65−66, and 182−183) have increased mobility on the picosecond to nanosecond time scale compared to the core of the aged cutinase−TC4 complex. The flexibility of the N-terminus appears to be highly restricted. Only 12 residues needed fitting with an exchange contribution. Except for Gly^{174}, the exchange terms are very small and there are no contiguous stretches of residues fitted with an exchange contribution, which indicates that the aged cutinase−TC4 complex exhibits no significant conformational exchange on the microsecond to millisecond time scale.

The overall rotational correlation time of the complex is 1 ns shorter than the overall rotational correlation time of

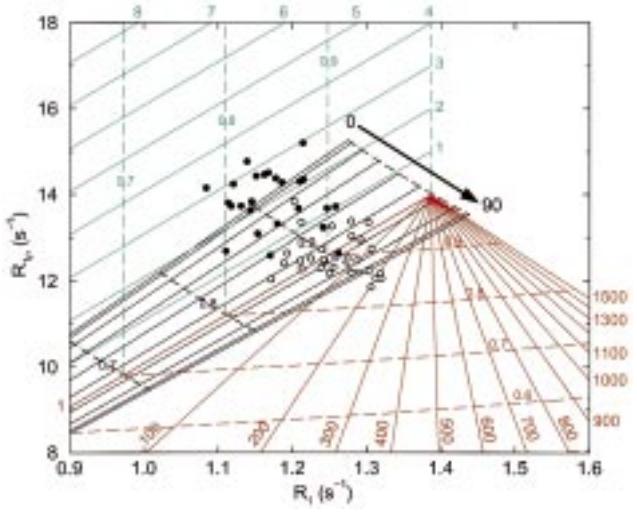

FIGURE 5: Experimental R_1 and $R_{1\rho}$ combinations of the aged cutinase−TC4 complex for residues in two major α-helices (53−63 and 92−108; filled circles), with their N−H vectors running nearly parallel to the long axis of the molecule, and for residues in the β-sheet (34−39, 68−72, 113−119, 141−147, and 167−170; open circles), with their N−H vectors nearly orthogonal to the long axis of the molecule. The experimental values are covered by a grid of R_1 and $R_{1\rho}$ combinations predicted for a protein with an (effective) overall rotational correlation time of 9.68 ns. Combinations of R_1 and $R_{1\rho}$ values are given for different values of (1) S^2 and the internal correlation time (τ_e) when isotropic tumbling is assumed (in red; isotropic model 2), (2) S^2 and the exchange contribution (R_{ex}) when isotropic tumbling is assumed (in green; isotropic model 3), and (3) S^2 and the angle between the N−H internuclear vector and the unique axis of the molecule (θ) when anisotropic rotational diffusion is taken into account with a ratio $D_\parallel/D_\perp$ of 1.3 (in black; anisotropic model 1). The red lines represent different values of τ_e (indicated in picoseconds by the red numbers), the green lines represent different R_{ex} values (indicated in s^{-1} by the green numbers), and the black lines represent different values of θ. The black arrow runs from $\theta = 0°$ to 90°, for which the curves are drawn at intervals of 10°. The dashed lines connect equal S^2 values (indicated by the smaller numbers) at 0.1 intervals. The point at which all red lines coincide is the isotropic, completely rigid situation ($S^2 = 1$).

the free enzyme from *E. coli* (9.82 versus 10.80 ns; ref *32*). This is most probably due to the absence of the N-terminal propeptide in the complex. In the free enzyme, the highly flexible propeptide most likely protrudes into the solvent and is strongly hydrated, which might slow the molecular tumbling. Apart from this propeptide, the regions which are mobile on the picosecond to nanosecond time scale are comparable for the aged cutinase−TC4 complex and the free enzyme. However, for the free enzyme 30 more residues needed fitting with an exchange term compared to the complex. These residues were mainly located in loops, including the second binding loop, in the flap helix 81−85, and in one of the outer strands as well as at the N-terminal side of the β-sheet. The microsecond to millisecond mobility observed in these regions in the free enzyme has nearly vanished upon inhibition.

Comparison of R_2 and $R_{1\rho}$. For the aged cutinase−TC4 complex the differences between R_2 and $R_{1\rho}$ are small and only for Ser^{91} this difference exceeds 4 s^{-1} (Figure 7). For free cutinase, as many as 28 residues were shown to have $R_2 - R_{1\rho}$ values larger than 4 s^{-1} (*14*). These residues are all located in the binding site of the enzyme (Figure 7), and their high $R_2 - R_{1\rho}$ values were attributed to conformational exchange processes on a time scale slower than the frequency of the $R_{1\rho}$ spin-lock field (∼2.7 kHz), that is, the millisecond time scale (*14*). For the $R_{1\rho}$ measurements on the complex, the spin-lock power was nearly the same (∼2.6 kHz) and therefore the observed millisecond mobility in the free enzyme seems to be almost completely frozen upon inhibition. The higher $R_2 - R_{1\rho}$ value of Ser^{91} indicates that, only in the loop following the flap helix 81−85, there might remain some mobility on the millisecond time scale.

Analysis of Water-NOESY and Water-ROESY Spectra. In the water-ROESY spectra, the positive cross-peaks correspond to NHs which are in fast exchange with H_2O, while negative cross-peaks correspond to NHs in spatial proximity to bound H_2O or a rapidly exchanging hydroxyl proton. In the water-NOESY spectra, both types of cross-peaks are positive. Because $R_{1\rho}$ is much larger than R_1 for the amide protons, the water-ROESY spectra are inherently less sensitive than the water-NOESY spectra. For a number of residues the ROESY signals were indeed below the level of detection, whereas their NOESY peaks were well observable. It was therefore not possible to determine for all residues whether the magnetization transfer was caused by exchange or by cross-relaxation from the sign of their ROESY signals. However, for most of the residues without observable ROESY peaks, the mechanism of magnetization transfer could be deduced from the ratio of the water-NOESY signal intensities at 20 and 25 °C. The intensity of cross-peaks due to fast exchange should decrease when the temperature is lowered, as the rates of exchange decrease approximately 3-fold with every 10 °C decrease in temperature (*53*). In contradistinction, cross-peaks due to cross-relaxation will be stronger or about equally intense, because τ_c increases when the temperature is lowered.

Analogous to the free enzyme (*14*), only for a few residues in the aged cutinase−TC4 complex could exchange peaks be observed: Gly^{82}, Arg^{88}, Thr^{173}, and Gly^{174}. It can be shown that the amide protons of these residues should exchange faster than their intrinsic exchange rates (*14*, *52*). Gly^{82} is positioned at the N-terminus of the flap helix 81−85, and Arg^{88} is located in the loop following this flap helix. For the free enzyme an exchange peak was observed for Gly^{82} as well, but the amide signal of Arg^{88} was broadened beyond detection, which precluded the detection of fast exchange for this residue. However, for free cutinase exchange peaks were observed for Ser^{92} and Ala^{93}, which are positioned in the same loop, but these residues do not give rise to exchange signals in the water-NOESY spectra of the complex. One of the explanations for the exchange peaks of Gly^{82}, Ser^{92}, and Ala^{93} in the spectra of the free enzyme was the large amplitude millisecond time scale mobility of the loops connecting the flap helix to the core of the protein. This argument does not seem to hold for the complex (vide supra), and that would be in agreement with the absence of exchange peaks for Ser^{92} and Ala^{93}. The exchange of Gly^{82} could, however, still be enhanced by the flap helix dipole, and for Arg^{88} it could be accelerated by its positively charged side chain. The exchange peaks for Thr^{173} and Gly^{174} were also observed for the free enzyme and can be explained by conformational exchange processes: Gly^{174} has a very large exchange contribution to its R_2 and $R_{1\rho}$ (see Figure 4). This implies that it adopts multiple conformations, which interconvert on a time scale faster than 2.6 kHz. No attempt was

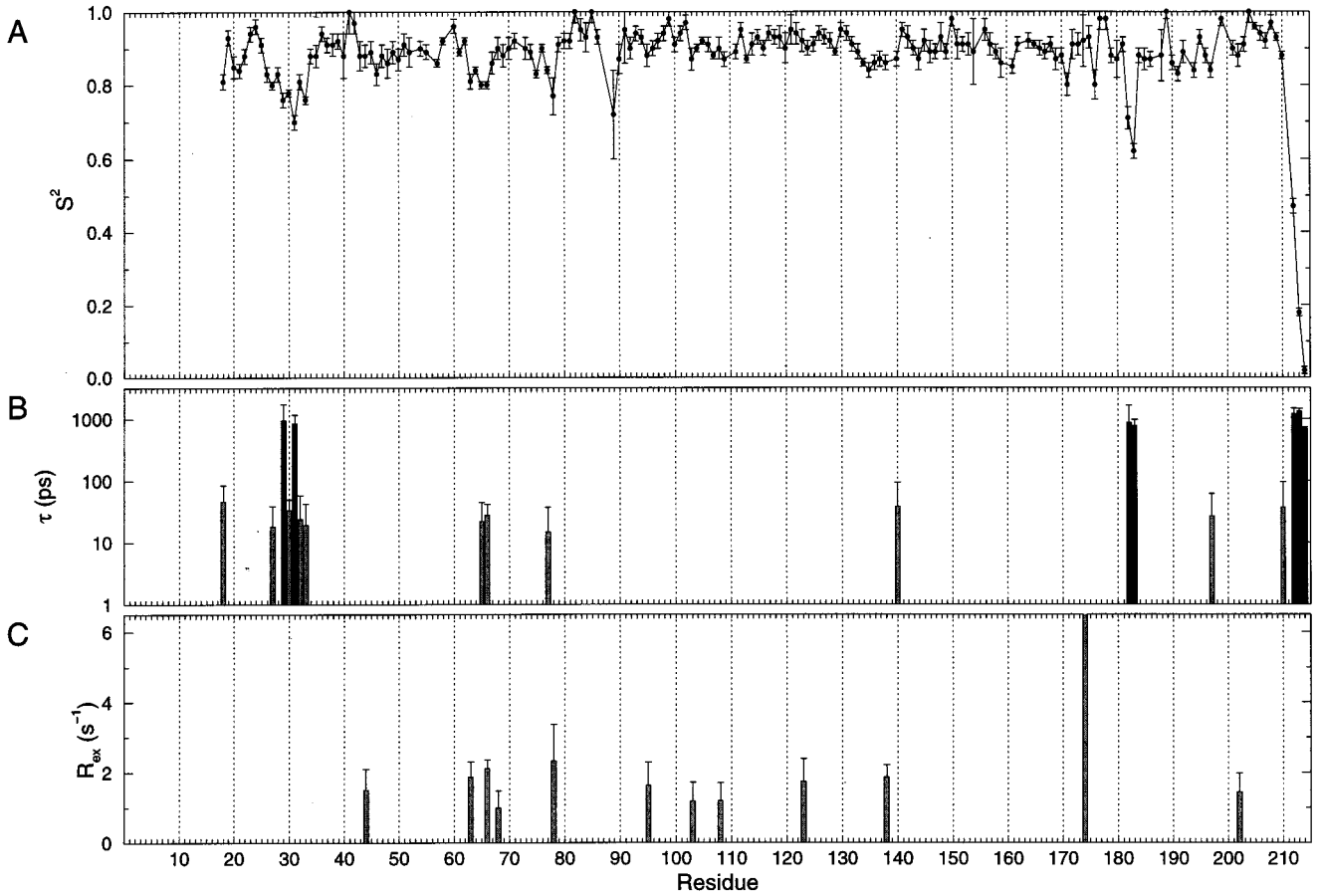

FIGURE 6: Model-free parameters of the aged cutinase−TC4 complex when including anisotropy at an optimized τ_c of 9.82 ns: (A) generalized order parameter S^2, (B) internal correlation times τ_e (gray bars) and τ_s (black bars), and (C) exchange contribution to R_2 and $R_{1\rho}$. The exchange contribution of residue 174 runs off the scale, but was 12.56 ± 2.34 s^{-1}.

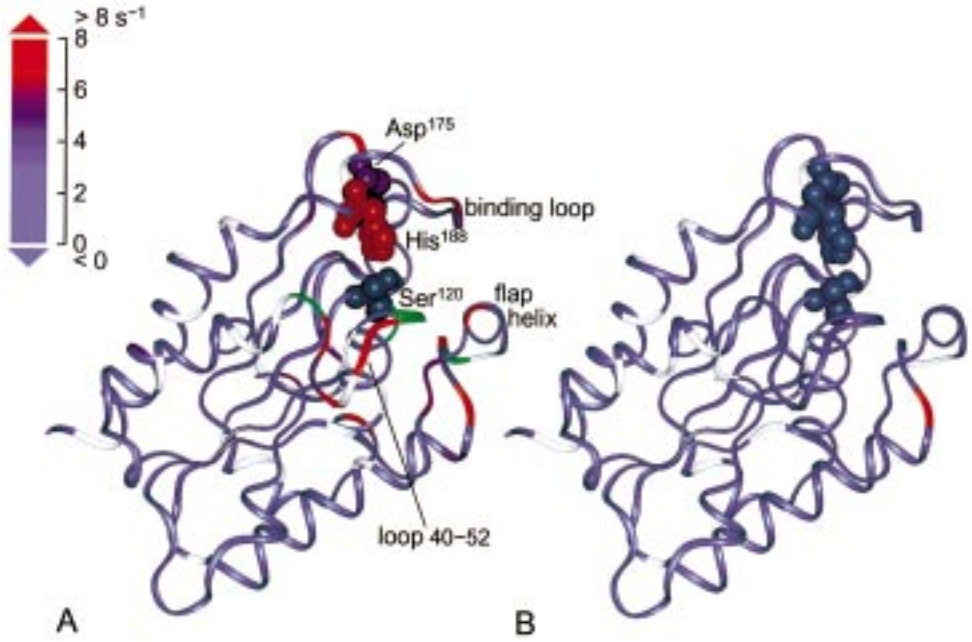

FIGURE 7: Differences between the ^{15}N R_2 and $R_{1\rho}$ relaxation rates for (A) free cutinase (*14*) and (B) the aged cutinase−TC4 complex, mapped on the crystal structure of the free protein (*5*). The five residues which have not been assigned in the free enzyme, Ser^{42}, Thr^{43}, Thr^{50}, Arg^{88}, and Gln^{121}, are colored green in part A. Prolines, residues with overlapping signals, and the N-terminal arginine in part B, for which the difference could not be determined, are colored white. The active site residues are shown in space-filling representations. This figure was generated with the program Insight II (MSI).

made to quantify the exchange rate constants for the residues with exchange peaks.

As a NOE/ROE to water cannot be distinguished from a NOE/ROE to a rapidly exchanging hydroxyl proton resonat-

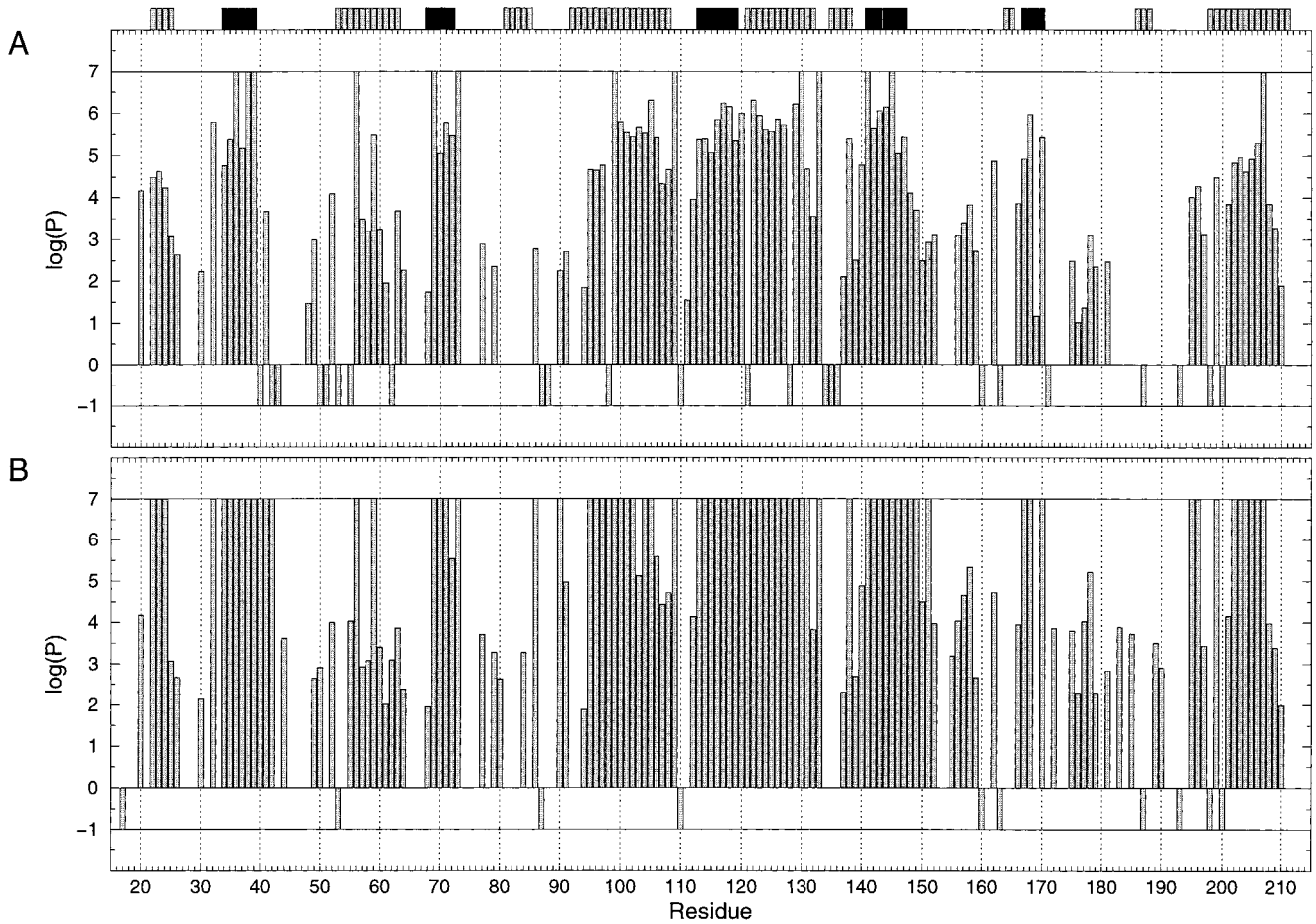

FIGURE 8: Amide hydrogen protection factors for (A) free cutinase (*14*) and (B) the aged cutinase−TC4 complex. A log(*P*) of 0 was assigned to residues which exchanged too fast to be measured, and a log(*P*) of 7 was assigned to residues which did not exchange significantly after (A) one month or (B) one week. Prolines, residues with missing assignments or overlapping signals in part A, and the N-terminal arginine in part B, for which the protection factor could not be determined, were given a log(*P*) of −1. Residues in β-strands and helices are indicated by the black and gray bars, respectively, at the top of the figure.

ing at the H_2O chemical shift (*54*), the proximity to hydroxyl groups of serines, threonines, and tyrosines was checked for each amide proton in the crystal structure of the cutinase−TC4 complex (*11*). All side chains of aspartic and glutamic acids were assumed to be deprotonated at the pH of the sample used for the measurements. Among the residues showing cross-relaxation signals in the water-NOESY spectra of the aged cutinase−TC4 complex, 10 residues could be identified of which the amide protons give an unambiguous NOE to bound water: Arg^{40}, Gly^{41}, Val^{73}, Asn^{152}, Leu^{153}, Ile^{159}, Leu^{176}, Val^{177}, Gly^{180}, and Ala^{185}. These are exactly the same residues which were shown to bind water molecules in the free enzyme (*14*), except for Arg^{40}, whose amide signal had overlap in the HSQC spectrum of free cutinase. For the free enzyme one additional contacting residue could be identified, Gln^{154}, which did not give rise to a NOE peak in the water-NOESY spectra of the complex. The NMR data can be fully explained using the five water molecules which were shown to bind to the free enzyme in solution as well, and which are present in the crystal structures of both free cutinase (*5*) and the cutinase−TC4 complex (*11*).

Protection Factors. Amide hydrogen protection factors in the aged cutinase−TC4 complex are plotted in Figure 8. All major secondary structural elements are protected from exchange, while the loop regions in general exchange much faster. The central β-sheet is almost completely protected from exchange. Helix 53−63 shows an amphipathic character, while the other protected helices are more uniformly protected.

For comparison, the protection factors in the free enzyme (*14*) are also shown in Figure 8. The regions which are protected in both the complex and the free enzyme are very similar. For the free enzyme, exchange data were collected until one month after dissolving the protein in D_2O, while the complex data were collected only until one week after dissolving the material in D_2O. This explains why more high protection factors could be determined for free cutinase. A number of residues in the binding region are more protected in the complex compared to the free enzyme: 41, 44, 80, 84, 86, 90, 91, 149−152, 155−158, 172, 175−178, 183, 185, 189, and 190. This indicates that the binding site is more stable in the inhibited enzyme. Noteworthy, the amides of Ser^{42} and Gln^{121}, which together with the O^{γ} atom of Ser^{42} form the oxyanion hole, are protected from exchange in the cutinase−inhibitor complex. The amides of these residues are two of the resonances which could not be identified for free cutinase, which indicated that the oxyanion hole is not preformed in the free enzyme in solution (*13*). In the complex, the oxyanion hole appears to be rigidly formed, with the amides of Ser^{42} and Gln^{121} hydrogen bonded to the oxygen atom of the inhibitor, which prevents them from exchanging with the solvent.

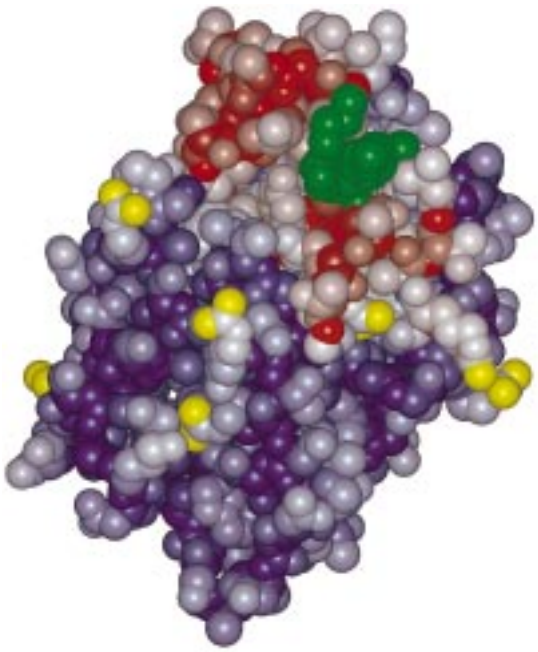

FIGURE 9: Weighted averages of the differences in amide ^{1}H and ^{15}N chemical shifts between the fresh and the aged cutinase−TC4 complex, mapped on a CPK model of the crystal structure of the cutinase−TC4 complex (*11*) according to the coloring scheme described in the Materials and Methods section. The arginine $N^{\eta 1}$ and $N^{\eta 2}$ atoms are colored yellow. The inhibitor is shown in green. This figure was generated with the program Insight II (MSI).

DISCUSSION

The X-ray structure of the cutinase−TC4 complex (*11*) did not provide an explanation for the effect of the chain length at the 1-position on the activity, neither could it explain the enantioselectivity of the enzyme (*19*), because the chains at the 1- and 2-positions protrude from the protein. In the crystal structure, two cutinase−TC4 complex molecules face each other head-to-head and part of the inhibitor has interactions with the neighboring cutinase molecule and its bound inhibitor. The observed conformation might thus be an artifact of the crystallization process. In solution, the cutinase−TC4 complex is monomeric and the conformation found in the protein crystal would be highly unfavorable.

The amide chemical shift differences between the fresh and the aged cutinase−TC4 complex are directly caused by the presence or absence of the dicarbamoyl-glycerol moiety, which is split off during the aging process, and may thus yield information on the position of (one of) the two carbamoyl chains in solution. However, these differences might also be caused by a conformational change induced by the dicarbamoyl-glycerol part of the inhibitor and should therefore be interpreted with great care. The large shifts in the second binding loop (Figure 3C) suggest that this loop might accommodate (one of) the two carbamoyl chains. In Figure 9 two regions can be identified which, on the basis of the amide chemical shift differences, are most likely to make contact with a carbamoyl chain. The figure suggests that, in solution, the inhibitor is bound in a tuning fork conformation. The exact positions of the carbamoyl chains remain unclear, but it seems that they nestle up to the protein's surface and retain some conformational freedom. NOEs between the protein and the carbamoyl chains of the inhibitor would give direct evidence for their positions in solution. Unfortunately, no NOEs could be observed between the cutinase amide protons and the carbamoyl chain protons in the ^{15}N-edited forward/backward NOESY spectrum. This is probably due to the hydrophobic nature of these chains, which will preferentially make contact with the hydrophobic amino acid side chains of the protein. If cutinase isotopically enriched with ^{13}C and a triglyceride analogue, which forms a more stable complex, were available, it would be possible to determine the structure of the complex in solution.

Another interesting feature noted from Figure 9 is that a number of arginine residues are located just below the regions which seem to make contact with the carbamoyl chains. The arginine side chains constitute a positively charged collar, which is assumed to prevent aggregation at the hydrophobic binding region (*55*). Our results confirm the view that, when the enzyme adsorbs to a lipid layer, the binding region is immersed in the lipidic phase, while the positively charged collar just remains in the water phase.

While the amide resonances of the residues in the binding site of cutinase shift significantly upon inhibitor binding, the resonances in the core of the protein appear to be hardly affected (Figures 3A,B). This is in agreement with our previous findings, from which it was concluded that the core of cutinase forms the stable scaffold for its catalytic apparatus (*14*). However, inhibitor binding has a large effect on the internal backbone mobility of cutinase, which is not confined to the binding site. In the free enzyme, the internal mobility at the C-termini of the β-strands was almost completely restricted, while the N-termini of the strands seemed to allow somewhat more flexibility on the microsecond to millisecond time scale (*14*). In the aged cutinase−TC4 complex, this mobility at the N-terminal side of the β-sheet has completely disappeared (Figure 6). Thus, inhibitor binding even influences the internal dynamics of that part of the enzyme opposite to the binding site.

Residues 27−33 and 65−66, two loop regions outside the binding region, show some increased flexibility on the picosecond to nanosecond time scale (Figure 6), just like in the free enzyme (*14*). The increased flexibility of loop 27−33 seemed to be interrupted at Ala^{32} in the free molecule, which was attributed to the amide−aromatic hydrogen bond between Ala^{32} and the aromatic ring of Trp^{69} (*13*). In the complex, Ala^{32} appears to be involved in the picosecond to nanosecond motions as well. This questions whether the amide−aromatic hydrogen bond has the stabilizing function suggested before (*14*).

The microsecond to millisecond time scale mobility present in the binding site of free cutinase is mostly frozen in the aged cutinase−TC4 complex. Loop 40−52 was found to be highly mobile on the millisecond time scale in the free enzyme (*14*). It contains Ser^{42}, of which the main-chain nitrogen and the O^{γ} atom form the oxyanion hole together with the main-chain nitrogen of Gln^{121}. The amide resonances of Ser^{42}, Thr^{43}, and Thr^{50} in this loop and of Gln^{121} were not identified for the free enzyme (*13*), which indicated that the oxyanion hole is rather flexible in solution (*14*). For the complex, all of these signals could be observed (Figure 2) and the millisecond mobility of loop 40−52 has completely disappeared (Figure 7). Furthermore, the amides of the oxyanion hole residues Ser^{42} and Gln^{121} are protected from exchange (Figure 8). These results show that, while the oxyanion hole was flexible in the free enzyme in solution,

it is rigidly formed in the complex with a substrate-like inhibitor.

The millisecond mobility of the loops (residues 73−80 and 86−91) connecting the flap helix 81−85 to the core observed for the free enzyme (*14*), has, except for Ser[91], disappeared in the complex (Figure 7). The amide signal of Arg[88], which was broadened beyond detection in the free enzyme (*13*), could be observed in the complex (Figure 2). In free cutinase, loops 73−80 and 86−91 performed a hinge function, moving the flap helix as a whole, thereby opening and closing the binding site like in a true lipase. The reorientations of this helix probably led to the exchange contributions to the $R_{1\rho}$ of nearly all residues in helix 81−85 in the free enzyme. In agreement with the rigidification of the loops, these exchange contributions are absent for the flap helix in the complex (Figure 6).

Except for Gly[174], all microsecond to millisecond mobility in the second binding loop 171−191, which contains the active site residues Asp[175] and His[188], as observed for the free enzyme (*14*) has disappeared in the complex (Figures 6 and 7). Just like in the free enzyme, Gly[174] has a rather extreme exchange contribution to its R_2 and $R_{1\rho}$ (Figure 4). Together with residue 173, it gives rise to exchange peaks in the water-NOESY spectra. We have no explanation for these phenomena. Residues 182 and 183 display mobility on the picosecond to nanosecond time scale (Figure 6). This flexibility in the tip of the second binding loop was also present in the free molecule (*14*) and might only be restricted in the intact, fresh complex.

The fact that for the aged as well as for the fresh complex all amide signals could be observed, while for the free enzyme five signals were broadened beyond detection (*13*), already indicates that both complexes are rigidified compared to the free protein. The line widths of the amide signals for the aged and the fresh complex are roughly the same, which indicates that there are no large differences in the backbone dynamics of the two complexes. Apparently, the binding of the chain at the 3-position not only rigidifies the flap helix, but also decreases the mobility of the other binding loop. This binding loop is not directly involved in binding the chain at the 3-position. It contains the active site Asp[175] and His[188], which are flexible in the free enzyme, but fixed into their proper positions in the aged complex. Apparently, these two residues constrain the microsecond to millisecond mobility of the whole binding loop, even when only a very small inhibitor is bound.

The five bound water molecules in the collar around the binding site, where the oil−water interface is expected to be in heterogeneous reactions, detected for the free enzyme (*14*) are also present in the aged cutinase−TC4 complex. During binding to an interface, these water molecules might be displaced as the environment becomes more hydrophobic, but apparently they do not interfere with inhibitor binding.

The dynamical studies performed on free cutinase and the aged cutinase−TC4 complex show that in solution the enzyme adopts its active conformation only upon binding of the inhibitor. While the active site Ser[120] is rigidly attached to the stable α/β core of the protein, the remainder of the binding site is very flexible in the free enzyme. The other two active site residues Asp[175] and His[188] as well as the oxyanion hole residues Ser[42] and Gln[121] are only restrained into their proper positions upon binding of the substrate-like inhibitor. The flap helix, which opens and closes the binding site in the free molecule, is also fixed in the cutinase−inhibitor complex. Our results are in contrast with the X-ray analysis results, namely that in the protein crystal, free cutinase has a well-defined active site and a preformed oxyanion hole (*5*, *6*) and that it does not need any rearrangements to bind its substrate (*6*, *11*). Our solution studies show that cutinase does need conformational rearrangements to bind its substrate, which may form the rate-limiting step in catalysis.

ACKNOWLEDGMENT

We thank E.-J. Rutjes and M. C. D. van der Burg-Koorevaar for the production and purification of the uniformly ^{15}N-labeled cutinase, S. de Jong for help with the SAS package, C. J. van Platerink and P. J. W. Schuyl for the electrospray mass spectrometry, and J. de Vlieg for stimulating discussions.

SUPPORTING INFORMATION AVAILABLE

A table with the amide resonance assignments of the aged and the fresh cutinase−TC4 complex, a table containing the backbone ^{15}N R_1, R_2, and $R_{1\rho}$ relaxation rates and the heteronuclear NOEs of the aged cutinase−TC4 complex, tables with the parameters as obtained from the model-free analyses using both the isotropic and the anisotropic model, and four supplementary figures. The figures contain bar charts of the weighted averages of the differences in amide ^{1}H and ^{15}N chemical shifts, graphs of the model-free parameters of the aged cutinase−TC4 complex when assuming isotropic tumbling at an optimized τ_c of 9.68 ns, graphs of the model-free parameters of free cutinase when including anisotropy at an optimized τ_c of 10.80 ns, and bar charts of the differences between the ^{15}N R_2 and $R_{1\rho}$ relaxation rates for free cutinase and the aged cutinase−TC4 complex, respectively. This material is available free of charge via the Internet at http://pubs.acs.org.

REFERENCES

1. Kolattukudy, P. E. (1984) in *Lipases* (Borgström, B., and Brockman, H. L., Ed.) pp 471−504, Elsevier, Amsterdam, The Netherlands.
2. de Geus, P., Lauwereys, M., and Matthyssens, G. (1990) *World Patent WO 90/09446*.
3. Lauwereys, M., de Geus, P., de Meutter, J., Stanssens, P., and Matthyssens, G. (1991) in *Lipases: Structure, Mechanism and Genetic Engineering* (Alberghina, L., Schmid, R. D., and Verger, R., Eds.) Vol. 16, pp 243−251, VCH, Weinheim, Germany.
4. Verger, R. (1997) *Trends Biotechnol. 15*, 32−38.
5. Martinez, C., de Geus, P., Lauwereys, M., Matthyssens, G., and Cambillau, C. (1992) *Nature 356*, 615−618.
6. Martinez, C., Nicolas, A., van Tilbeurgh, H., Egloff, M.-P., Cudrey, C., Verger, R., and Cambillau, C. (1994) *Biochemistry 33*, 83−89.
7. Longhi, S., Czjzek, M., Lamzin, V., Nicolas, A., and Cambillau, C. (1997) *J. Mol. Biol. 268*, 779−799.
8. Brzozowski, A. M., Derewenda, U., Derewenda, Z. S., Dodson, G. G., Lawson, D. M., Turkenburg, J. P., Bjorkling, F., Huge-Jensen, B., Patkar, S. A., and Thim, L. (1991) *Nature 351*, 491−494.
9. Derewenda, U., Brzozowski, A. M., Lawson, D. M., and Derewenda, Z. S. (1992) *Biochemistry 31*, 1532−1541.
10. van Tilbeurgh, H., Egloff, M.-P., Martinez, C., Rugani, N., Verger, R., and Cambillau, C. (1993) *Nature 362*, 814−820.

11. Longhi, S., Mannesse, M., Verheij, H. M., de Haas, G. H., Egmond, M., Knoops-Mouthuy, E., and Cambillau, C. (1997) *Protein Sci. 6*, 275−286.
12. Brünger, A. T. (1997) *Nat. Struct. Biol. 4*, 862−865.
13. Prompers, J. J., Groenewegen, A., van Schaik, R. C., Pepermans, H. A. M., and Hilbers, C. W. (1997) *Protein Sci. 6*, 2375−2384.
14. Prompers, J. J., Groenewegen, A., Hilbers, C. W., and Pepermans, H. A. M. (1999) *Biochemistry 38*, 5315−5327.
15. Mannesse, M. L. M., Boots, J.-W. P., Dijkman, R., Slotboom, A. J., van der Hijden, H. T. W. M., Egmond, M. R., Verheij, H. M., and de Haas, G. H. (1995) *Biochim. Biophys. Acta 1259*, 56−64.
16. Berends, F., Posthumus, C. H., v. d. Sluys, I., and Deierkauf, F. A. (1959) *Biochim. Biophys. Acta 34*, 576−578.
17. Michel, H. O., Hackley, B. E., Jr., Berkowitz, L., List, G., Hackley, E. B., Gillilan, W., and Pankau, M. (1967) *Arch. Biochem. Biophys. 121*, 29−34.
18. Lang, D. A., Mannesse, M. L. M., de Haas, G. H., Verheij, H. M., and Dijkstra, B. W. (1998) *Eur. J. Biochem. 254*, 333−340.
19. Mannesse, M. L. M., Cox, R. C., Koops, B. C., Verheij, H. M., de Haas, G. H., Egmond, M. R., van der Hijden, H. T. W. M., and de Vlieg, J. (1995) *Biochemistry 34*, 6400−6407.
20. van Gemeren, I. A., Musters, W., van den Hondel, C. A. M. J. J., and Verrips, C. T. (1995) *J. Biotechnol. 40*, 155−162.
21. Nicolas, A., Egmond, M., Verrips, C. T., de Vlieg, J., Longhi, S., Cambillau, C., and Martinez, C. (1996) *Biochemistry 35*, 398−410.
22. Glasoe, P. K., and Long F. A. (1960) *J. Phys. Chem. 64*, 188−190.
23. Marion, D., Ikura, M., Tschudin, R., and Bax, A. (1989) *J. Magn. Reson. 85*, 393−399.
24. Mori, S., Abeygunawardana, C., Johnson, M. O., and van Zijl, P. C. M. (1995) *J. Magn. Reson., Ser. B 108*, 94−98.
25. Talluri, S., and Wagner, G. (1996) *J. Magn. Reson., Ser. B 112*, 200−205.
26. Jahnke, W., Baur, M., Gemmecker, G., and Kessler, H. (1995) *J. Magn. Reson., Ser. B 106*, 86−88.
27. Fulton, D. B., Hrabal, R., and Ni, F. (1996) *J. Biomol. NMR 8*, 213−218.
28. Kay, L. E., Torchia, D. A., and Bax, A. (1989) *Biochemistry 28*, 8972−8979.
29. Boyd, J., Hommel, U., and Campbell, I. D. (1990) *Chem. Phys. Lett. 175*, 477−482.
30. Kay, L. E., Nicholson, L. K., Delaglio, F., Bax, A., and Torchia, D. A. (1992) *J. Magn. Reson. 97*, 359−375.
31. Palmer, A. G., III, Skelton, N. J., Chazin, W. J., Wright, P. E., and Rance, M. (1992) *Mol. Phys. 75*, 699−711.
32. Prompers, J. J., Groenewegen, A., de Jong, S., Hilbers, C. W., and Pepermans, H. A. M. (submitted for publication).
33. Bax, A., and Pochapsky, S. S. (1992) *J. Magn. Reson. 99*, 638−643.
34. Piotto, M., Saudek, V., and Sklenář, V. (1992) *J. Biomol. NMR 2*, 661−665.
35. Messerle, B. A., Wider, G., Otting, G., Weber, C., and Wüthrich, K. (1989) *J. Magn. Reson. 85*, 608−613.
36. Wider, G., Riek, R., and Wüthrich, K. (1996) *J. Am. Chem. Soc. 118*, 11629−11634.
37. Marion, D., Ikura, M., and Bax, A. (1989) *J. Magn. Reson. 84*, 425−430.
38. Zhu, G., and Bax, A. (1990) *J. Magn. Reson. 90*, 405−410.
39. Grzesiek, S., Bax, A., Hu, J.-S., Kaufman, J., Palmer, I., Stahl, S. J., Tjandra, N., and Wingfield, P. T. (1997) *Protein Sci. 6*, 1248−1263.
40. Marquardt, D. W. (1963) *J. Soc. Ind. Appl. Math. 11*, 431−441.
41. Press, W. H., Flannery, B. P., Teukolsky, S. A., and Vetterling, W. T. (1986) *Numerical Recipes − The Art of Scientific Computing*, Cambridge University Press, Cambridge, U.K.
42. Peng, J. W., Thanabal, V., and Wagner, G. (1991) *J. Magn. Reson. 95*, 421−427.
43. Peng, J. W., and Wagner, G. (1994) *Methods Enzymol. 239*, 563−596.
44. Peng, J. W., and Wagner, G. (1994) in *NMR Probes of Molecular Dynamics* (Tycko, R., Ed.) pp 373−454, Kluwer Academic Publishers, Dordrecht, The Netherlands.
45. Davis, D. G., Perlman, M. E., and London, R. E. (1994) *J. Magn. Reson., Ser. B 104*, 266−275.
46. Lipari, G., and Szabo, A. (1982) *J. Am. Chem. Soc. 104*, 4546−4559.
47. Lipari, G., and Szabo, A. (1982) *J. Am. Chem. Soc. 104*, 4559−4570.
48. Clore, G. M., Driscoll, P. C., Wingfield, P. T., and Gronenborn, A. M. (1990) *Biochemistry 29*, 7387−7401.
49. Clore, G. M., Szabo, A., Bax, A., Kay, L. E., Driscoll, P. C., and Gronenborn, A. M. (1990) *J. Am. Chem. Soc. 112*, 4989−4991.
50. Fushman, D., Weisemann, R., Thüring, H., and Rüterjans, H. (1994) *J. Biomol. NMR 4*, 61−78.
51. Tjandra, N., Kuboniwa, H., Ren, H., and Bax, A. (1995) *Eur. J. Biochem. 230*, 1014−1024.
52. Bai, Y., Milne, J. S., Mayne, L., and Englander, S. W. (1993) *Proteins: Struct., Funct., Genet. 17*, 75−86.
53. Scholtz, J. M., and Robertson, A. D. (1995) *Methods Mol. Biol. 40*, 291−311.
54. Otting, G., and Wüthrich, K. (1989) *J. Am. Chem. Soc. 111*, 1871−1875.
55. Egmond, M. R., van der Hijden, H. T. W. M., Musters, W., Peters, H., Verrips, C. T., and de Vlieg, J. (1994) *World Patent WO 94/14963*.

BI990039K